Activation cross-sections of deuteron induced nuclear reactions on neodymium up to 50 MeV

F. Tárkányi[a], S. Takács[a], F. Ditrói[a,*], A. Hermanne[b], H. Yamazaki[c], M. Baba[c], A. Mohammadi[c], A.V. Ignatyuk[d]

[a]*Institute for Nuclear Research, Hungarian Academy of Sciences (ATOMKI), Debrecen, Hungary*
[b]*Cyclotron Laboratory, Vrije Universiteit Brussel (VUB), Brussels, Belgium*
[c]*Cyclotron Radioisotope Center (CYRIC), Tohoku University, Sendai, Japan*
[d]*Institute of Physics and Power Engineering (IPPE), Obninsk, Russia*

arXiv:1411.2760v1 [nucl-ex] 11 Nov 2014

Abstract

In the frame of a systematic study of activation cross sections of deuteron induced nuclear reactions on rare earths, the reactions on neodymium for production of therapeutic radionuclides were measured for the first time. The excitation functions of the ^{nat}Nd(d,x) ^{151,150,149,148m,148g,146,144,143}Pm, ^{149,147,139m}Nd, ^{142}Pr and ^{139g}Ce nuclear reactions were assessed by using the stacked foil activation technique and high resolution γ-spectrometry. The experimental excitation functions were compared to the theoretical predictions calculated with the modified model codes ALICE-IPPE-D and EMPIRE-II-D and with the data in the TENDL-2012 library based on latest version of the TALYS code. The application of the data in the field of medical isotope production and nuclear reaction theory is discussed.

Keywords: Nd target, deuteron activation, Pm, Nd and Ce radioisotopes, yield curves

1. Introduction

Activation cross-sections data of deuteron induced nuclear reactions on neodymium are important for development of nuclear reaction theory and for different practical applications. This study was performed in the frame of the following ongoing research goals:

- To check the predictive power and benchmarking of the different model codes of the nuclear reaction theory. To contribute to the improvement of models for description of deuteron induced reactions and to selection of more appropriate input parameters.
- To investigate the alternative production possibilities of standard and emerging therapeutic and diagnostic lanthanide radionuclides via charged particle induced reactions. In a search for new nuclides suitable for therapeutic purposes [1–8] the radionuclide ^{149}Pm ($T_{1/2}$ = 53.1 h), ^{141}Nd ($T_{1/2}$) and ^{140}Nd ($T_{1/2}$ = 3.37 d), were found to offer some unique properties suitable for therapy and the daughter nuclide ^{140}Pr ($T_{1/2}$ = 3.4 min) brings the additional advantage of in-vivo localization via positron emission tomography (PET).
- To contribute to the extension of the database by a systematic study of activation cross-sections of deuteron induced nuclear reactions for biological and industrial applications (accelerator technology, thin layer activation, activation in space technology, etc.).

Here we present our results on activation cross-sections on deuteron induced nuclear reactions on neodymium. No earlier experimental data on ^{nat}Nd were found in the literature. Only one earlier set of experimental cross-section data was found on highly enriched ^{148}Nd for investigation the isomeric ratios of the (d,2n) reactions [9]. Thick target yield data for production of ^{143,144,148}Pm at 22 MeV were reported by Dmitriev et al. at 22 MeV [10].

2. Experiment and data evaluation

For measurements, the well-known activation method, stacked foil irradiation technique and high resolution γ-spectrometry was used. Nd metal foils and NdO pellet targets, interleaved with Al foils for monitoring of beam characteristics, were stacked and irradiated at CYRIC (Sendai) and UCL (LLN) cyclotrons. Complete excitation function was measured

*Corresponding author: ditroi@atomki.hu

for the monitor reactions to control the beam intensity and the energy. The main experimental parameters, methods of data evaluation are collected in Table 1 and Table 2. The comparison of the re-measured monitor reactions and the recommended data are shown in Fig. 1. The decay characteristics of the investigated reaction products and the possibly contributing reactions in the energy region studied are summarized in Table 3.

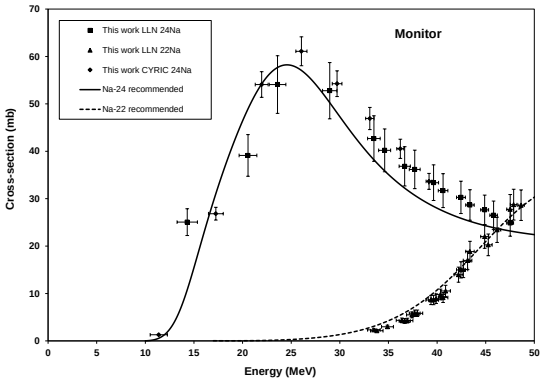

Figure 1: Comparison of the measured and the recommended cross-sections or the used monitor ^{27}Al(d,x)^{22,24}Na reactions

3. Comparison with the results of the model codes

The cross-sections of the investigated reactions were calculated using the modified model codes ALICE-IPPE [20] and EMPIRE-II [19]. In the used modified ALICE-IPPE-D and EMPIRE-D code versions the direct (d,p) channel is increased strongly [20, 21]. The experimental data are also compared with the cross-section data reported in the TALYS based [22] TENDL-2012 Data Libraries [23].

4. Results

4.1. Cross-sections

The cross-sections for all the reactions investigated are shown in Figs. 215 and the numerical values are collected in Table 4-5. The results of the two irradiations on different targets are given separately allowing to judge on the agreement in the overlapping energy range. We should mention, as is reflected in the figures that the experimental results of this investigations have larger uncertainties and the data are more scattered, than in most of our previous investigations. Taking into accounts that the scattering shows a systematic behavior between the two experiments, it could be connected to the target thicknesses. In the LLN experiment a large metal foil was used and the average thickness was derived from measurements of the surface of the whole foil and its weight. The final targets were obtained by cutting pieces of the required dimensions from the large foil. Due to the well-known oxidation problems the thickness of each individual target piece were not re-measured but supposed to be equal to the average. In the Sendai experiment the Nd2O3 targets were made by pressing neodymium oxide in a precisely machined Al cup. The average thickness of each individual targets was derived on the basis the measured oxide weight (total weight minus weight of Al-cup) and known surface, but the uniformity of the targets was only roughly checked. For both experiments the beam diameter was significantly lower than the diameter of the targets and hence possible local changes in thickness can result in large scattering of cross-section data.

4.1.1. Production cross-sections of ^{151}Pm (cum)

The ^{151}Pm ($T_{1/2}$=28.40 h) is produced directly via ^{150}Nd(d,n) reaction and from the decay of short-lived ^{151}Nd ($T_{1/2}$ = 12.44 min) obtained in a ^{150}Nd(d,p) reaction. Due to the experimental circumstances we could only measure the cumulative production after the complete decay of the short-lived parent. As it is shown in Fig. 2 the experimental data are in acceptable agreement with the results of ALICE-D and EMPIRE-D, but in case of TENDL-2012 the underestimation is very significant.

4.1.2. Production cross-sections of ^{150}Pm

For ^{150}Pm ($T_{1/2}$ = 2.68 h) we have experimental data only from the 50 MeV irradiation due to the long cooling time (19 h) of the first series of measurement in the 40 MeV experiment. The ^{150}Pm can only be produced via the ^{150}Nd(d,2n) reaction. The measured data and the theoretical model calculations are shown in Fig. 3. The agreement between the experimental and theoretical results is acceptable.

4.1.3. Production cross-sections of ^{149}Pm

The experimental and theoretical excitation functions of ^{149}Pm ($T_{1/2}$ = 53.08 h) are shown in Fig. 4. Two reactions are contributing on stable Nd isotopes with approximately the same natural abundance (^{148}Nd(d,n) and ^{150}Nd(d,3n)). The maximum around 20 MeV (seen

Table 1: Main experimental parameters

Incident particle	Deuteron	Deuteron
Method	Stacked foil	Stacked foil
Target composition	^{nat}Nd (100 μm)-target ^{nat}Yb (22.88 μm)-target Al (49.06 μm)-monitor (repeated 11 times) Interleaved with Al (156.6 μm, 103.43 μm, 49.06 μm)-energy degraders	74.7-93.7 μm Nd_2O_3 target pressed into 360 μm thick Al backing covered by 10 μm Al foil
Number of Nd target foils	11	8
Accelerator	Cyclone 110 cyclotron of the Universit Catholique in Louvain la Neuve (LLN) Belgium	AVF-930 cyclotron of the Cyclotron and Radioisotope Center (CYRIC) of Tohoku University in Sendai, Japan
Primary energy	50 MeV	40 MeV
Covered energy range	49.4-21.5 MeV	39.4-9.7 MeV
Irradiation time	60 min	20 min
Beam current	92 nA	45 nA
Monitor reaction, [recommended values]	^{27}Al(d,x)^{24}Na reaction [11] (re-measured over the whole energy range)	^{27}Al(d,x)^{24}Na reaction (re-measured over the whole energy range)
Monitor target and thickness	^{nat}Al, 49.06 mm	^{nat}Al, 370 mm target holders
detector	HPGe	HPGe
Chemical separation	no	no
g-spectra measurements	4 series	3 series
Typical cooling times (and target-detector distances)	3 h (35 cm) 34 h (10 cm) 47 h (20 cm) 272 (5cm)	19 h (10 cm) 90 h (10 cm) 600 h (10 cm)

Table 2: Main parameters and methods of the data evaluation (with references)

Gamma spectra evaluation	Genie 2000, Forgamma	[11, 12]
Determination of beam intensity	Faraday cup (preliminary) Fitted monitor reaction (final)	[13]
Decay data (see Table 2)	NUDAT 2.6	[14]
Reaction Q-values (see Table 3)	Q-value calculator	[15]
Determination of beam energy	Andersen (preliminary) Fitted monitor reaction (final)	[16] [14]
Uncertainty of energy	Cumulative effects of possible uncertainties (primary energy, target thickness, energy straggling, correction to monitor reaction)	
Cross-sections	Isotopic and elemental cross-sections	
Uncertainty of cross-sections	sum in quadrature of all individual contributions (beam current (7%), beam-loss corrections (max. of 1.5%), target thickness (1%), detector efficiency (5%), photo peak area determination counting statistics (1-20 %)	[17]
Yield	Physical yield	[18]

in the experiment and confirmed by the theoretical predictions) indicates that the cross-sections for the (d,3n) reaction are significantly higher than those for (d,n).

4.1.4. Production cross-sections of ^{148m}Pm

The measured excitation functions came in all cases from a combination of (d,xn) reactions on the ^{185}Re and ^{187}Re. The level schemes for ^{182}Re and ^{184}Re are estimated with large uncertainties for some important γ-transitions. So, an accuracy of calculations for the corresponding isomer yields cannot be very high.

The ^{148}Pm has two long-lived isomeric states. The ^{148m}Pm ($T_{1/2}$ = 41.29 d) higher laying state shows only for a small part isomeric decay (IT: 4.2 %) and emits strong, independent γ-lines allowing separate identification. The agreement of our 2 data points below 18 MeV with the data of [9] is reasonable. The theoretical data overestimate the experimental values (Fig. 5). The maxima of the two contributing reactions ((d,2n) and (d,4n)) are well pronounced in the figure, especially for the model calculations.

4.1.5. Production cross-sections of ^{148g}Pm

The cross-sections for the direct production of the ^{148g}Pm ($T_{1/2}$ = 5.368 d) (after correction for the small contribution of the ^{148m}Pm decay) are shown in Fig. 6 in comparison with the earlier experimental data and the theoretical predictions. The overestimation by the theory for production of the ground state is significant. Our experimental results below 18 MeV for production of the ground and metastable state are not detailed enough to allow any calculation of isomeric ratio and comparison with [9].

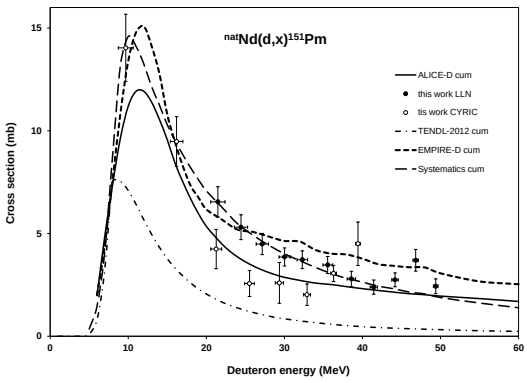

Figure 2: Experimental cross-sections for the ^{nat}Nd(d,x)^{151}Pm reaction and comparison with the theoretical code calculations

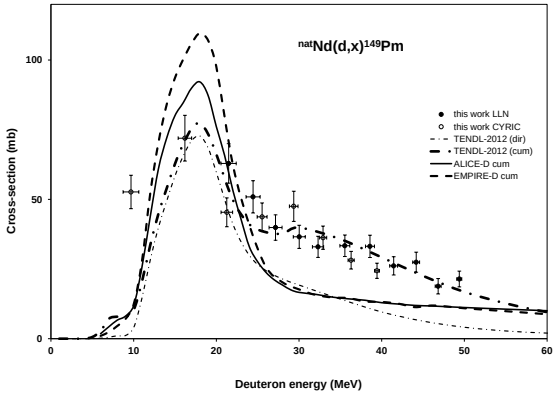

Figure 4: Experimental cross-sections for the ^{nat}Nd(d,x)^{149}Pm reaction and comparison with the theoretical code calculations

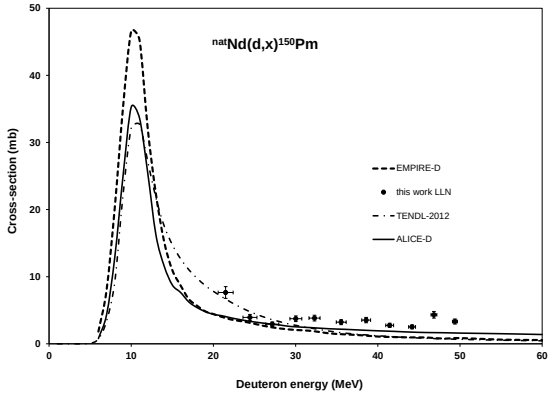

Figure 3: Experimental cross-sections for the ^{nat}Nd(d,x)^{150}Pm reaction and comparison with the theoretical code calculations

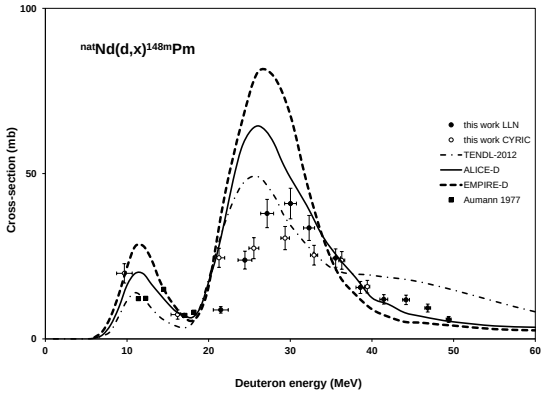

Figure 5: Experimental cross-sections for the ^{nat}Nd(d,x)^{148m}Pm reaction and comparison with the theoretical code calculations

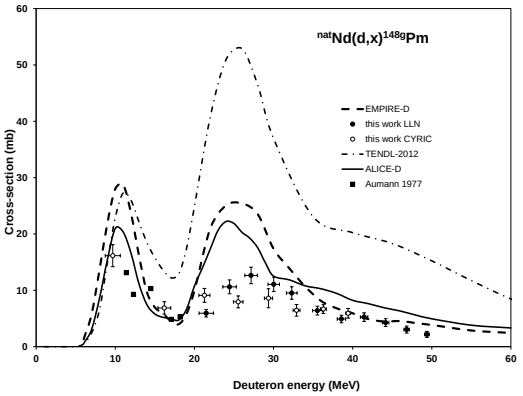

Figure 6: Experimental cross-sections for the ^{nat}Nd(d,x)^{148g}Pm reaction and comparison with the theoretical code calculations

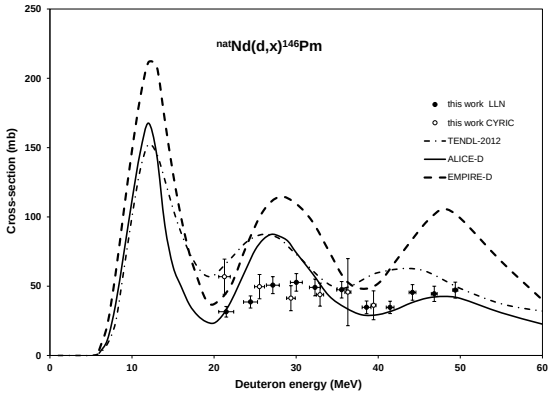

Figure 7: Experimental cross-sections for the ^{nat}Nd(d,x)^{146}Pm reaction and comparison with the theoretical code calculations

4.1.6. Production cross sections of ^{147}Pm

Due to the long half-life ($T_{1/2}$ = 2.62 a) and the very low abundance of its unique -line this industrially important radionuclide could not be detected, neither as directly produced nor as decay product of its parent ^{147}Nd.

4.1.7. Production cross-sections of ^{146}Pm

The comparison of the experimental and the theoretical data of the ^{146}Pm ($T_{1/2}$ = 5.53 a) shows significant overestimation of the experiment by the used models that however clearly show the contributions of different stable target isotopes (Fig. 7).

4.1.8. Production cross-sections of ^{144}Pm

The ^{144}Pm ($T_{1/2}$ = 363 d) is produced by (d,xn) reactions on 143-^{150}Nd isotopes of ^{nat}Nd. The shape of the excitation function predicted in TENDL-2012 differs significantly from the predictions of the ALICE-D and EMPIRE-D and from the experiment, especially at the high energy range (Fig. 8).

4.1.9. Production cross-sections of ^{143}Pm

The (d,xn) reactions on all stable isotopes of ^{nat}Nd participate in the production of the ^{143}Pm ($T_{1/2}$ = 265 d). The comparison of the experiment and the theory shows a similar picture as for previous cases: the experimental data are overestimated by the theory and are not distinguishing well the different contributing reactions (Fig. 9).

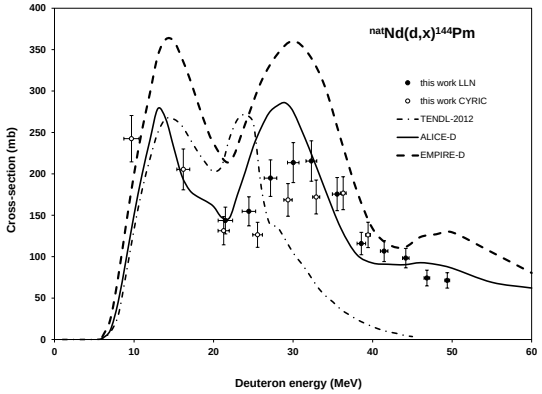

Figure 8: Experimental cross-sections for the ^{nat}Nd(d,x)^{144}Pm reaction and comparison with the theoretical code calculations

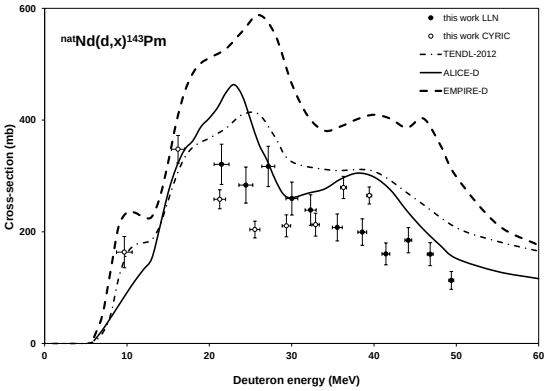

Figure 9: Experimental cross-sections for the ^{nat}Nd(d,x)^{143}Pm reaction and comparison with the theoretical code calculations

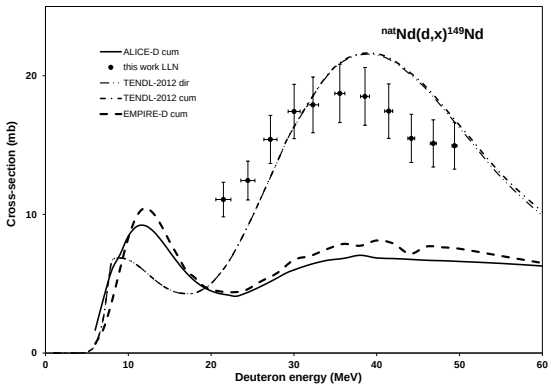

Figure 10: Experimental cross-sections for the ^{nat}Nd(d,x)^{149}Nd reaction and comparison with the theoretical code calculations

4.1.10. Production cross-sections of ^{149}Nd(cum)

Due to the long cooling time for the 40 MeV experiment (around 19 h) we could not measure the cross-sections for production of ^{149}Nd ($T_{1/2}$ = 1.728 h) in this experiment. The measured cross-sections for the 50 MeV experiment (Fig. 10) represent cumulative production of ^{149}Nd directly by (d,pxn) and from the complete β^--decay of the short-lived ^{149}Pr ($T_{1/2}$ = 2.26 min). The two maxima seen on the theoretical excitation functions correspond to the ^{148}Nd(d,p) and ^{150}Nd(d,p2n) reactions. The contribution from the decay of ^{149}Pr is negligible, according to the TENDL-2012 results and is only visible at energies above 50 MeV. There are large disagreements in the theoretical predictions. The predictions of the (d,p) part are more reliable in case of ALICE-D and EMPIRE-D, but the (d,p2n) energy range is strongly underestimated by these codes. In the measured energy region the TENDL-2012 results are more close to the experiment.

4.1.11. Production cross-sections of ^{147}Nd(cum)

The production cross-sections of ^{147}Nd ($T_{1/2}$ = 10.98 d) were deduced from spectra taken after complete decay of short-lived parent ^{147}Pr ($T_{1/2}$ = 13.4 min) and hence represent cumulative production (direct + decay from parent). The first maximum (Fig. 11) represents the (d,p) contribution on ^{146}Nd, where the description of the ALICE-D and EMPIRE-D is better. It is difficult to compare the experimental data with the theory in the higher energy range.

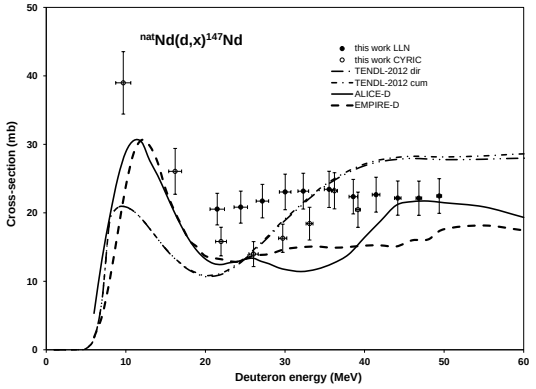

Figure 11: Experimental cross-sections for the ^{nat}Nd(d,x)^{147}Nd reaction and comparison with the theoretical code calculations

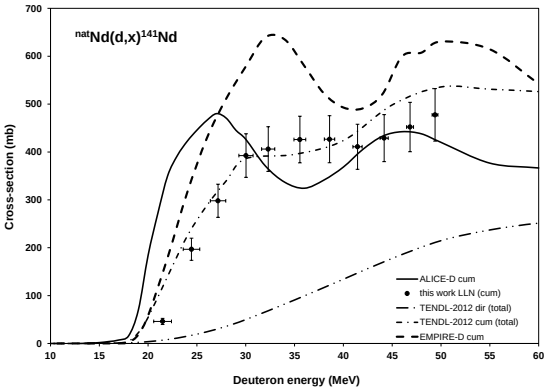

Figure 12: Experimental cross-sections for the ^{nat}Nd(d,x)^{141}Nd reaction and comparison with the theoretical code calculations

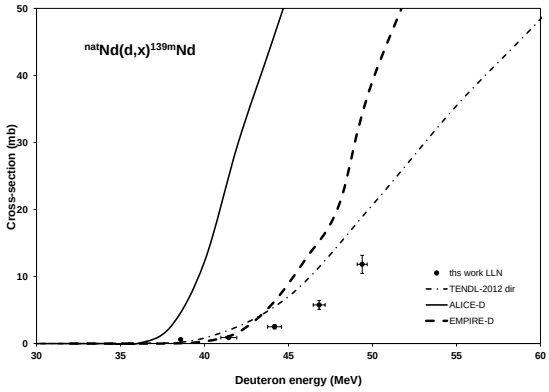

Figure 13: Experimental cross-sections for the ^{nat}Nd(d,x)^{139m}Nd reaction and comparison with the theoretical code calculations

4.1.12. Production cross-sections of ^{141}Nd(cum)

The short-lived isomeric state ($T_{1/2}$ = 62.0 s) of ^{141}Nd is decaying with IT (100 %) to the ground state ($T_{1/2}$ = 2.49 h). The ground state of ^{141}Nd is also fed by EC + β^+-decay of ^{141}Pm (20.90 min) and is produced directly by (d,pxn) reactions on all stable Nd isotopes. The measured cross-sections for the production of the ground state are cumulative, including all above mentioned contributions (Fig. 12). According to the Fig. 12 there are very large disagreements between the predictions of the different theoretical codes and the experimental data.

4.1.13. Production cross-sections of ^{139m}Nd

The ^{139}Nd has two long-lived isomeric states, the (I^π = 3/2$^+$, $T_{1/2}$ = 29.7 min) ground state and the longer-lived high spin metastable state (I^π = 11/2$^-$, $T_{1/2}$ = 5.50 h). We obtained cross-sections for production of the high spin state that is produced only directly via (d,pxn) reactions. The ^{139}Pm (I^π = 5/2$^+$, $T_{1/2}$ = 4.15 min) decays only to the ground state of 139Nd. Our experimental data (Fig. 13) are closer to the TALYS predictions in the TENDL-2012 than to the ALICE-D and EMPIRE-D results.

4.1.14. Production cross-sections of ^{142}Pr

We could deduce a few experimental cross-section data for production of the ^{142}Pr ($T_{1/2}$ = 19.12 h) radioisotope, only obtained directly via (d,2pxn) reactions. The comparison with the theoretical predictions is shown in Fig. 14.

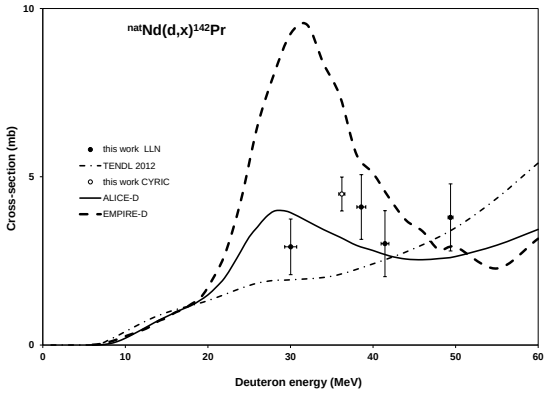

Figure 14: Experimental cross-sections for the ^{nat}Nd(d,x)^{142}Pr reaction and comparison with the theoretical code calculations.

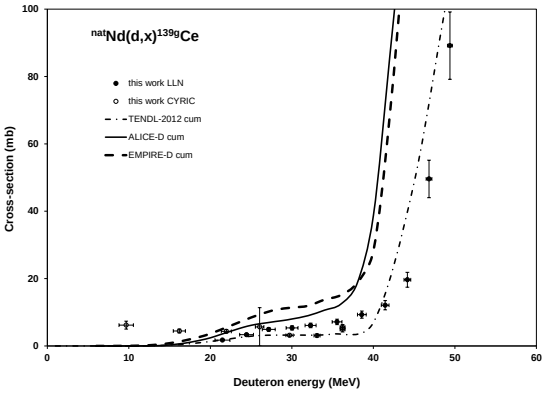

Figure 15: Experimental cross-sections for the ^{nat}Nd(d,x)^{139g}Ce reaction and comparison with the theoretical code calculations.

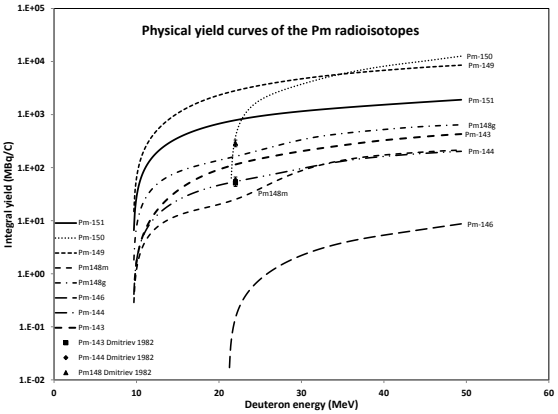

Figure 16: Physical yields of the Pm radioisotopes

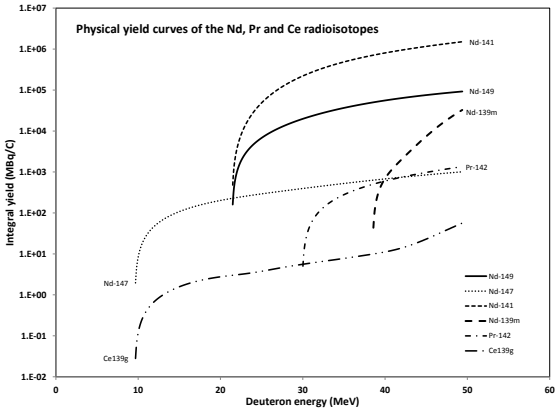

Figure 17: Physical yields of the Nd, Pr and Ce radioisotopes

4.1.15. Production cross-sections of ^{139g}Ce(cum)

The direct production cross-sections of the long-lived ^{139}Ce ($T_{1/2}$ = 137.641 d) via (d,3pxn) reactions are very small. The main contributions to the measured cumulative cross-sections arise from the shorter-lived ^{139}Pm-^{139}Nd-^{139}Pr decay chain. Among the used theoretical results the TENDL-2012 data agree rather well with the experimental cumulative excitation function (see Fig. 15).

4.2. Integral yields

The integral yields (integrated yield for a given incident energy down to the reaction threshold), calculated from tted curves to our experimental cross-section data, are shown in Fig. 16-17 in comparison with experimental thick target yields found in the literature. The results are representing so called physical yields (obtained in an instantaneous irradiation time for an incident number of particles having charge equivalent to 1 Coulomb)[18]. Fig. 16 also contains the data from Dmitriev [10] measured at 22 MeV, where the result for ^{144}Pm is in excellent agreement with our measurement, while his results for ^{143}Pm and ^{148}Pm are above and below our curves respectively.

5. Summary and conclusion

Activation cross-sections of proton induced nuclear reactions on neodymium were measured for the ^{nat}Nd(d,x) ^{151,150,149,148m,148g,146,144,143}Pm, ^{149,147,139m}Nd,

^{142}Pr and ^{139g}Ce nuclear reactions. All investigated reactions are presented here for the first time, except the data of [9] for the ^{148}Nd(d,2n) reaction. Model calculations were done by using the EMPIRE-D and AICE-IPPE-D codes. The data were also compared with the data of the TALYS based TENDL-2012 online library. The predictions of theoretical calculations are only moderately successful. The obtained experimental data provide a basis for upgrading the model codes and input parameters. As it was mentioned the data can be used for selection and optimization of production routes for the medically relevant radioisotopes ^{149}Pm ($T_{1/2}$ = 53.1 h), ^{141}Nd (2.49 h) and ^{140}Nd ($T_{1/2}$=3.37 d).

6. Acknowledgements

This work was done in the frame MTA-FWO research project and ATOMKI-CYRIC collaboration. The authors acknowledge the support of research projects and of their respective institutions in providing the materials and the facilities for this work.

References

[1] G. Stocklin, S. M. Qaim, F. Rosch, The impact of radioactivity on medicine, Radiochimica Acta 70-1 (1995) 249–272.

[2] S. M. Qaim, Therapeutic radionuclides and nuclear data, Radiochimica Acta 89 (4-5) (2001) 297–302.

[3] M. Neves, A. Kling, A. Oliveira, Radionuclides used for therapy and suggestion for new candidates, Journal of Radioanalytical and Nuclear Chemistry 266 (3) (2005) 377–384.

[4] H. Uusijarvi, P. Bernhardt, T. Ericsson, E. Forssell-Aronsson, Dosimetric characterization of radionuclides for systemic tumor therapy: Influence of particle range, photon emission, and subcellular distribution, Medical Physics 33 (9) (2006) 3260–3269.

[5] G. J. Beyer, Radioactive ion beams for biomedical research and nuclear medical application, Hyperfine Interactions 129 (1-4) (2000) 529–553.

[6] F. Rosch, Radiolanthanides in endoradiotherapy: an overview, Radiochimica Acta 95 (6) (2007) 303–311.

[7] M. R. Zalutsky, Radionuclide therapy, Vol. 4, Springer, 2011, p. 2180.

[8] H. Uusijarvi, P. Bernhardt, F. Rosch, H. R. Maecke, E. Forssell-Aronsson, Electron- and positron-emitting radiolanthanides for therapy: Aspects of dosimetry and production, Journal of Nuclear Medicine 47 (5) (2006) 807–814.

[9] D. C. Aumann, W. Guckel, Absolute cross-sections and isomeric cross-section ratios for nd-148(d,2n), nd-148(p,n), and nd-146(alpha,pn) reactions producing isomeric pair pm-148(m,g), Physical Review C 16 (1) (1977) 160–166.

[10] P. P. Dmitriev, N. N. Krasnov, G. A. Molin, Radioactive nuclide yields for thick target at 22 mev deuterons energy, Yadernie Konstanti 34 (4) (1982) 38.

[11] Canberra, http://www.canberra.com/products/radiochemistry_lab-/genie-2000-software.asp. (2000).

[12] G. Székely, Fgm - a flexible gamma-spectrum analysis program for a small computer, Computer Physics Communications 34 (3) (1985) 313–324.

[13] F. Tárkányi, F. Szelecsényi, S. Takács, Determination of effective bombarding energies and fluxes using improved stacked-foil technique, Acta Radiologica, Supplementum 376 (1991) 72.

[14] R. R. Kinsey, C. L. Dunford, J. K. Tuli, T. W. Burrows, Nudat 2.6 http://www.nndc.bnl.gov/nudat2/, in: Proceedings of the 9th International Symposium on Capture Gamma Ray Spectroscopy and Related Topics, Vol. 2, Springer Hungarica Ltd, p. 657.

[15] B. Pritychenko, A. Sonzogni, Q-value calculator, http://www.nndc.bnl.gov/qcalc (2003).

[16] H. H. Andersen, J. F. Ziegler, Hydrogen stopping powers and ranges in all elements. The stopping and ranges of ions in matter, Volume 3., The Stopping and ranges of ions in matter, Pergamon Press, New York, 1977.

[17] I.-B. of-Weights-and Measures, Guide to the expression of uncertainty in measurement, 1st Edition, International Organization for Standardization, Genve, Switzerland, 1993.

[18] M. Bonardi, The contribution to nuclear data for biomedical radioisotope production from the milan cyclotron facility (1987).

[19] M. Herman, R. Capote, B. V. Carlson, P. Oblozinsky, M. Sin, A. Trkov, H. Wienke, V. Zerkin, Empire: Nuclear reaction model code system for data evaluation, Nuclear Data Sheets 108 (12) (2007) 2655–2715.

[20] F. Tárkányi, A. Hermanne, S. Takács, F. Ditrói, I. Spahn, S. F. Kovalev, A. V. Ignatyuk, S. M. Qaim, Activation cross sections of the tm-169(d,2n) reaction for production of the therapeutic radionuclide yb-169, Applied Radiation and Isotopes 65 (6) (2007) 663–668.

[21] F. Tárkányi, A. Hermanne, S. Takács, K. Hilgers, S. F. Kovalev, A. V. Ignatyuk, S. M. Qaim, Study of the 192os(d,2n) reaction for, production of the therapeutic radionuclide 192ir in no-carrier added form, Applied Radiation and Isotopes 65 (11) (2007) 1215–1220.

[22] A. J. Koning, S. Hilaire, M. C. Duijvestijn, Talys-1.0 (2007).

[23] A. J. Koning, D. Rochman, S. van der Marck, J. Kopecky, J. C. Sublet, S. Pomp, H. Sjostrand, R. Forrest, E. Bauge, H. Henriksson, O. Cabellos, S. Goriely, J. Leppanen, H. Leeb, A. Plompen, R. Mills, Tendl-2013: Talys-based evaluated nuclear data library (2012).

Table 3: Decay characteristic of the investigated reaction products and the contributing reactions

Nuclide Decay path	Half-life	E_γ(keV)	I_γ(%)	Contributing reaction	Q-value (keV)
^{151}**Pm** β^-: 100 %	28.40 h	240.09 340.08 445.68	3.8 22.5 4.0	^{150}Nd(d,n)	4770.71
^{150}**Pm** β^-: 100%	2.68 h	333.92 406.51 831.85 876.41 1165.77 1324.51	68 5.6 11.9 7.3 15.8 17.5	^{150}Nd(d,2n)	-3089.5
^{149}**Pm** b$^-$: 100%	53.08 h	285.95	3.1	^{148}Nd(d,n) ^{150}Nd(d,3n)	3720.27 -8693.63
^{148m}**Pm** IT: 4.2 % β^-: 95.8 %	41.29 d	432.745 550.284 629.987 725.673 915.331 1013.808	5.33 94.5 89 32.7 17.10 20.20	^{148}Nd(d,2n) ^{150}Nd(d,4n)	-3549.66 -15963.56
^{148g}**Pm** β^-: 100 %	5.368 d	550.27 914.85 1465.12	22.0 11.5 22.2	^{148}Nd(d,2n) ^{150}Nd(d,4n)	-3549.66 -15963.56
^{146}**Pm** ε: 66.0 %	5.53 a	453.88 735.93	65.0 22.5	^{145}Nd(d,n) ^{146}Nd(d,2n) ^{148}Nd(d,4n) ^{150}Nd(d,6n)	3086.77 -4478.47 -17103.16 -29517.07
^{144}**Pm** ε: 100 %	363 d	476.78 618.01 696.49	43.8 98 99.49	^{143}Nd(d,n) ^{144}Nd(d,2n) ^{145}Nd(d,3n) ^{146}Nd(d,4n) ^{148}Nd(d,6n) ^{150}Nd(d,8n)	2478.19 -5338.84 -11094.15 -18659.38 -31284.08 -43697.98
^{143}**Pm** ε: 100 %	265 d	741.98	38.5	^{142}Nd(d,n) ^{143}Nd(d,2n) ^{144}Nd(d,3n) ^{145}Nd(d,4n) ^{146}Nd(d,5n) ^{148}Nd(d,7n) ^{150}Nd(d,9n)	2074.99 -4048.59 -11865.62 -17620.92 -36201.1 -37810.85 -50224.76
^{149}**Nd** β^-: 100 %	1.728 h	114.314 211.309 270.166 326.554 423.553 540.509 654.831	19.2 25.9 10.7 4.56 7.4 6.6 8.0	^{148}Nd(d,p) ^{150}Nd(d,p2n) ^{149}Pr decay	2814.224 -9599.69 -12153.2
^{147}**Nd** β^-: 100 %	10.98 d	91.105 319.411 531.016	28.1 2.127 13.37	^{146}Nd(d,p) ^{148}Nd(d,p2n) ^{150}Nd(d,p4n) ^{147}Pr decay	3067.6343 -9557.07 -21970.98 4404.4
^{141}**Nd** ε: 100 %	2.49 h	145.45 1126.91 1147.30 1292.64	0.24 0.80 0.307 0.46	^{142}Nd(d,p2n) ^{143}Nd(d,p3n) ^{144}Nd(d,p4n) ^{145}Nd(d,p5n) ^{146}Nd(d,p6n) ^{148}Nd(d,p8n) ^{150}Nd(d,p10n) ^{141}Pm decay	-12052.37 -18175.95 -25992.98 -31748.28 -39313.52 -51938.22 -65222.22 -16505.2
^{139m}**Nd** ε: 88.2% IT: 11.8%	5.50 h	113.87 708.1 738.2 827.8 982.2	40 26 35 10.3 26	^{142}Nd(d,p4n) ^{143}Nd(d,p5n) ^{144}Nd(d,p6n) ^{145}Nd(d,p7n) ^{146}Nd(d,p8n) ^{139}Pm decay	-30373.8 -36497.3 -44314.4 -50069.7 -57634.9 -35670.2
^{142}**Pr** ε: 0.0164% β^-: 99.9836%	19.12 h	1575.6	3.7	^{142}Nd(d,2p) ^{143}Nd(d,2pn) ^{144}Nd(d,2p2n) ^{145}Nd(d,2p3n) ^{146}Nd(d,2p4n) ^{148}Nd(d,2p6n) ^{150}Nd(d,2p8n)	-3603.85 -9727.43 -17544.46 -23299.77 -30865.0 -43489.7 -55903.59
^{139}**Ce** e: 100%	137.641 d	165.8575	80	^{142}Nd(d,3p2n) ^{143}Nd(d,3p3n) ^{144}Nd(d,3p4n) ^{145}Nd(d,3p5n) ^{146}Nd(d,3p6n) ^{148}Nd(d,3p8n) ^{139}Pr decay	-23873.51 -29997.09 -37814.12 -43569.42 -51134.66 -63759.34 1510.73

When complex particles are emitted instead of individual protons and neutrons the Q-values have to be decreased by the respective binding energies of the compound particles: np-d, +2.2 MeV; 2np-t, +8.48 MeV

^{nat}Nd isotopic abundance: ^{142}Nd (27.13 %), ^{143}Nd (12.18 %), ^{144}Nd (23.80 %),^{145}Nd (5.30 %), ^{146}Nd (17.19 %), ^{148}Nd (5.76 %), ^{150}Nd (5.64 %)

Table 4: Measured cross-sections for production of the ^{151,150,149,148m,148g,146,144,143}Pm radionuclides

Energy (MeV)			^{151}Pm (mb)			^{150}Pm (mb)			^{149}Pm (mb)			^{148m}Pm (mb)			^{148g}Pm (mb)			^{146}Pm (mb)			^{144}Pm (mb)			^{143}Pm (mb)		
Sendai, 40 MeV																										
39.4	±	0.3	4.5	±	1.1				24.4	±	2.7	15.8	±	1.9	5.9	±	0.8	36.2	±	10.4	126	±	15	265	±	32
36.3	±	0.4	3.1	±	0.4				28.2	±	3.2	23.7	±	2.7	6.7	±	0.8	45.7	±	24.2	177	±	20	279	±	32
32.9	±	0.4	2.0	±	0.5				36.3	±	4.2	25.3	±	3.0	6.5	±	1.0	43.9	±	8.3	172	±	21	213	±	27
29.4	±	0.5	2.6	±	1.0				47.5	±	5.4	30.5	±	3.5	8.6	±	1.7	41.4	±	9.0	169	±	20	211	±	25
25.5	±	0.6	2.6	±	0.6				43.7	±	5.0	27.4	±	3.2	8.0	±	1.1	49.7	±	8.8	126	±	15	204	±	25
21.3	±	0.7	4.2	±	1.0				45.4	±	5.2	24.5	±	2.9	9.1	±	1.2	56.9	±	12.7	131	±	17	258	±	31
9.7	±	1.0	14.0	±	1.6				52.7	±	6.0	19.8	±	2.9	16.1	±	2.0				242	±	28	164	±	20
16.2	±	0.8	9.5	±	1.2				72.0	±	8.2	7.4	±	1.4	6.9	±	1.1				205	±	25	348	±	42
Louvain la Neuve, 50 MeV																										
49.4	±	0.3	2.4	±	0.4	3.3	±	0.4	21.4	±	2.8	5.9	±	0.9	2.2	±	0.5	47.2	±	5.8	71	±	9	113	±	16
46.8	±	0.4	3.7	±	0.5	4.3	±	0.5	18.8	±	2.8	9.3	±	1.2	3.0	±	0.6	44.5	±	5.5	74	±	9	160	±	21
44.2	±	0.4	2.7	±	0.3	2.5	±	0.3	27.4	±	3.6	11.8	±	1.4	4.3	±	0.7	45.5	±	5.6	98	±	12	185	±	23
41.4	±	0.5	2.4	±	0.3	2.7	±	0.3	26.1	±	3.3	12.0	±	1.4	5.3	±	0.8	34.7	±	4.5	107	±	13	160	±	20
38.6	±	0.5	2.8	±	0.4	3.5	±	0.4	33.1	±	4.0	15.6	±	1.8	4.9	±	0.7	34.8	±	4.6	116	±	14	199	±	24
35.5	±	0.6	3.5	±	0.4	3.2	±	0.4	33.4	±	3.9	24.4	±	2.8	6.4	±	0.8	47.4	±	5.9	176	±	20	208	±	24
32.3	±	0.7	3.7	±	0.4	3.8	±	0.4	33.0	±	3.8	33.6	±	3.8	9.5	±	1.1	49.1	±	6.0	215	±	24	239	±	27
30.0	±	0.7	3.9	±	0.4	3.7	±	0.4	36.6	±	4.2	40.9	±	4.6	11.1	±	1.3	52.7	±	6.3	214	±	24	260	±	30
27.2	±	0.8	4.5	±	0.5	2.9	±	0.3	39.9	±	4.6	37.9	±	4.3	12.6	±	1.5	50.7	±	6.1	195	±	22	317	±	36
24.4	±	0.8	5.3	±	0.6	3.9	±	0.4	50.9	±	5.8	23.8	±	2.7	10.6	±	1.2	38.6	±	4.4	155	±	18	284	±	32
21.5	±	0.9	6.5	±	0.7	7.6	±	0.9	62.9	±	7.1	8.8	±	1.0	5.9	±	0.7	31.6	±	3.8	144	±	16	321	±	36

Table 5: Measured cross-sections for production of the ^{149,147,139m}Nd, ^{142}Pr and ^{139g}Ce radionuclides

Energy (MeV)			^{149}Nd (mb)			^{147}Nd (mb)			^{141}Nd (mb)			^{139m}Nd (mb)			^{142}Pr (mb)			^{139g}Ce (mb)		
Sendai, 40 MeV																				
39.4	±	0.3				20.5	±	2.6										5.6	±	0.8
36.3	±	0.4				23.2	±	2.6										4.9	±	0.8
32.9	±	0.4				18.4	±	2.4										3.1	±	0.5
29.4	±	0.5				16.3	±	2.1										3.2	±	0.4
25.5	±	0.6				14.0	±	1.8										5.7	±	5.7
21.3	±	0.7				15.8	±	2.1										4.3	±	0.5
9.7	±	1.0				39.0	±	4.6										6.2	±	1.2
16.2	±	0.8				26.1	±	3.4										4.4	±	0.6
Louvain la Neuve, 50 MeV																				
49.4	±	0.3	15.0	±	1.7	22.5	±	2.5	478	±	55	11.82	±	1.35	3.79	±	1.00	89.2	±	10.0
46.8	±	0.4	15.1	±	1.7	22.1	±	2.5	452	±	52	5.76	±	0.65				49.6	±	5.6
44.2	±	0.4	15.5	±	1.7	22.2	±	2.5	429	±	49	2.50	±	0.31				19.7	±	2.2
41.4	±	0.5	17.4	±	2.0	22.7	±	2.6	411	±	47	0.89	±	0.14	3.01	±	0.98	12.1	±	1.4
38.6	±	0.5	18.5	±	2.1	22.4	±	2.5	427	±	49	0.59	±	0.10	4.10	±	0.96	9.3	±	1.1
35.5	±	0.6	18.7	±	2.1	23.4	±	2.6	426	±	49							7.1	±	0.8
32.3	±	0.7	17.9	±	2.0	23.2	±	2.6	406	±	47							6.1	±	0.7
30.0	±	0.7	17.4	±	2.0	23.1	±	2.6	393	±	45				2.92	±	0.83	5.4	±	0.6
27.2	±	0.8	15.4	±	1.7	21.7	±	2.4	298	±	35							4.9	±	0.6
24.4	±	0.8	12.4	±	1.4	20.8	±	2.3	197	±	23							3.3	±	0.4
21.5	±	0.9	11.1	±	1.2	20.5	±	2.3	46	±	6							1.7	±	0.2